Dalton Transactions

ROYAL SOCIETY OF CHEMISTRY

COMMUNICATION

View Article Online
View Journal | View Issue

Cite this: *Dalton Trans.*, 2024, **53**, 6860

Received 10th December 2023,
Accepted 1st April 2024

DOI: 10.1039/d3dt04123a

rsc.li/dalton

Field induced slow magnetic relaxation in a linear homotrinuclear manganese heterospin coordination compound with S = 7/2 ground state and intriguing spin density distribution†

Igor N. Shcherbakov, *[a] Ilya I. Krotkii,[a] Victoria I. Kazachkova,[a] Sergey N. Lyubchenko,[a] Nikolay N. Efimov,[b] Arshak A. Tsaturyan [c,d] and Vladimir A. Lazarenko [e]

We report a first example of field-induced (H_{DC} = 2500 Oe) slow magnetization relaxation in the homotrinuclear linear heterospin manganese coordination compound with S = 7/2 ground state, based on the bidentate 3,5-di-*tert*-butyl-1,2-benzoquinone-1-monooxime (HL) ligand with composition {[MnL_3]Mn[MnL_3]}.

Single molecule magnets (SMMs)[1–3] have attracted constant interest due to their potential technological applications[4–8] since the early 1990s. The first object with registered slow relaxation of magnetization was a well-known Mn_{12} complex.[9,10] So far, in the 3d-metal series SMM behaviour has been identified for Cr(II), Mn(III), Fe(III), Fe(II), Fe(I), Co(II), and Ni(II) systems.[11–13] From this point of view the Mn(II) ion as a potential SMM component is not promising. In a predominant number of compounds, it is in a high spin (HS) state with local S = 5/2, in which five 3d-electrons are distributed with close to spherical symmetry resulting in very small magnetic anisotropy. Nevertheless, a very scarce amount of mononuclear HS-Mn(II) compounds with slow relaxation of magnetization were reported recently.[14–17] High stability of the isotropic d^5 HS electronic state determines the fact that the local low spin (LS) state with S = 1/2 of Mn(II) is extremely rare. And even in the LS state Mn(II) is not a good SMM candidate because for S = 1/2 spin systems the magnetic anisotropy D parameter is undefined. SMM properties for Mn(II) compounds were reported earlier in the heteronuclear compounds with other metals, for example with lanthanides,[18,19] mixed valence Mn (II/III/IV), and Cu^{II}/Mn^{II}.[20] Homopolynuclear Mn(II) compounds with slow magnetization relaxation have not been reported to the best of our knowledge.

Reaction of 3,5-di-*tert*-butyl-1,2-benzoquinone-1-monooxime (**HL**)[21–23] with $Mn(ClO_4)_2 \cdot 6H_2O$ in a sealed ampule in isopropanol solution in the presence of triethylamine readily produced dark olive crystals with composition MnL_2, which appears to be the trinuclear coordination compound {[MnL_3]Mn[MnL_3]} (**1**) (see Scheme 1).

The synthetic procedure and characterization of **1** are detailed in the ESI.† A probable reaction mechanism is stepwise formation of anionic *fac*-$[MnL_3]^-$ units and further coordination of two $[MnL_3]^-$ anions by Mn^{2+} with formation of trinuclear compound **1**. An earlier analogous trinuclear Mn(II) compound was reported based on α-phenylazobenzaldehyde oxime as ligand.[24]

The structure of compound **1** was established with the single crystal X-ray diffraction (SCXRD) technique. The crystallographic parameters, structure refinement statistics and selected structural parameters for **1** are given in Tables S1 and S2, ESI.† The molecular structure of **1** is presented in Fig. 1. The formula unit corresponds to {[MnL_3]Mn[MnL_3]}. The compound is highly symmetric and belongs to the D_3 symmetry group. Three Mn ions lie on the C_3 symmetry axis (a view of the molecule along the C_3 axis is presented in Fig. S2, ESI†).

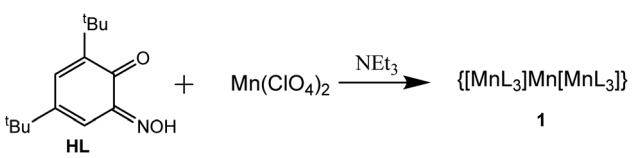

Scheme 1 Synthesis of compound **1**.

[a]*Southern Federal University, Chemistry Department, Rostov-On-Don, 344006, Russian Federation. E-mail: shcherbakov@sfedu.ru*
[b]*Kurnakov Institute of General and Inorganic Chemistry of the Russian Academy of Sciences, Moscow, 119991, Russian Federation*
[c]*Université Jean Monnet Saint-Etienne, CNRS, Institut d'Optique Graduate School, Laboratoire Hubert Curien UMR 5516, 42023 Saint-Étienne, France*
[d]*Institute of Physical and Organic Chemistry, Southern Federal University, 194/2 Stachka Ave., Rostov-On-Don, 344090, Russia*
[e]*National Research Center "Kurchatov Institute", Moscow, 123182, Russian Federation*

†Electronic supplementary information (ESI) available. CCDC 2284760. For ESI and crystallographic data in CIF or other electronic format see DOI: https://doi.org/10.1039/d3dt04123a

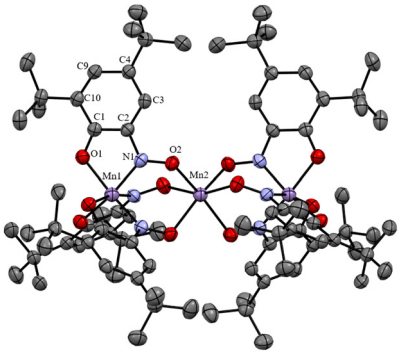

Fig. 1 Molecular structure of {[MnL_3]Mn[MnL_3]} (**1**) according to the SCXRD data (hydrogen atoms are not shown). Only symmetry non-equivalent atoms are labelled.

The middle manganese Mn2 atom is at the intersection point of the C_3 axis and three perpendicular C_2 axes (the angles between the C_2 axes are 60°). So, six $\mathbf{L}^-$ oximate ligands are symmetry equivalent, and both $[MnL_3]^-$ units are symmetry equivalent and, hence, so are both terminal manganese ions. The three linearly arranged Mn(II) cations are triply bridged by oximate N═O groups of the monodeprotonated ligands,[21,22] and the interatomic metal–metal distance is d(Mn1···Mn2) = 3.6153(13) Å. The terminal Mn centres are in a 3O3N distorted octahedral donor environment of three $\mathbf{L}^-$ ligands coordinated in a facial manner with oxygen O1 and nitroso nitrogen N1 atoms (CSM(OC-6) = 3.531, see Table S3, ESI†). The coordination bonds are rather short d(Mn1–O1) = 1.941(3) and d(Mn1–N1) = 1.912(3) Å, and noticeably differ in length (by *ca.* 0.03 Å).

The central Mn2 is in a trigonally distorted octahedral 6O coordination environment (CSM(OC-6) = 1.398, see Table S3, ESI†). Mn2 forms much longer equal Mn2–O2 bonds of 2.138 (3) Å, which are unambiguously falling in the range of Mn–O coordination bond lengths for Mn(II) in a local HS state. Short coordination bonds of Mn1(Mn1′) ions can arise for different reasons – firstly, due to the LS (S = 1/2) state of the terminal Mn(II) cations, and the $\{[Mn^{II-LS}L_3]Mn^{II-HS}[Mn^{II-LS}L_3]\}$ state of **1** or, secondly, due to intramolecular oxidation of Mn(II) to Mn(IV) by reduction of the two $\mathbf{L}^-$ ligands with formation of two dianion radical species (in analogy with close Mn coordination compounds with catecholate and semiquinonate radical ligands[25,26]) and the $[\{Mn^{IV}(L^{2\bullet-})_2(L^-)\}Mn^{II-HS}\{Mn^{IV}(L^{2\bullet-})_2(L^-)\}]$ state of **1**. In the latter case because of the high symmetry of molecule **1** charge (minus five) and spin density (two unpaired electrons) must be smeared over three ligands in each $[MnL_3]^-$ unit. It appeared to be hard to distinguish these cases based on solely structural data. Of course, intramolecular reduction of the ligand due to metal oxidation must pronouncedly influence the structure of the ligand, namely, the distribution of the bond lengths in the benzoquinone monooximate moiety. Such an influence, for example, for *N*-arylamidophenoxides of 3d metal complexes, was studied in ref. 27. For coordination compounds of benzoquinone monoxime derivatives such structural studies are not available. The problem for comparison of data in ref. 27 with structural data of the ligand in **1** is that the $\mathbf{L}^-$ anionic ligand is isoelectronic to neutral iminoquinone. One-electron reduction of $\mathbf{L}^-$ will lead to a dianion radical (isoelectronic to iminosemiquinone anion-radical) and two-electron reduction to the trianion (isoelectronic to dianion arylamidophenoxide). So, direct comparison of structural data for **L** in our case is not possible, because it involves species with different formal charges. To overcome this problem, the correlation coefficients between the lengths of C–C, C–N, and C–O bonds in the benzoquinone-monooxime moiety of **L** in **1** and average bond lengths in metal *N*-arylamidophenoxides with different ligand charges were calculated (see Table S5, ESI†). Close correlation coefficients were found for structural data of iminoquinone (oxidation state 0, r = 0.93) and iminosemiqinone (oxidation state −1, r = 0.95), indicating that it is not possible to unambiguously choose between the monoanionic or dianion radical state of the ligand **L** in the compound **1**.

The temperature dependence of molar magnetic susceptibility χ for compound **1** was measured in a static magnetic field of H_{DC} = 5000 Oe strength (see Fig. 2, reduced magnetisation and the low temperature region are shown in Fig. S3, ESI†).

The value of the χT product for complex **1** observed at 300 K is 7.08 cm^3 K mol^{-1}, which is much lower than the 13.125 cm^3 K mol^{-1} value expected for three independent Mn(II) ions in a local HS state assuming g = 2. So, the terminal Mn ions are for sure not in the d^5 HS state, as is supported by XRD data. If a proposition is made about the LS Mn(II) state of the terminal manganese centres, then the uncoupled value must be 5.125 cm^3 K mol^{-1}, significantly lower than the experimental value, but if ferromagnetic exchange interaction between Mn centres is considered sufficiently strong to keep a parallel arrangement of electrons at room temperature, then seven aligned electron spins give the theoretical χT value of 7.875 cm^3 K mol^{-1}, only slightly higher than the value

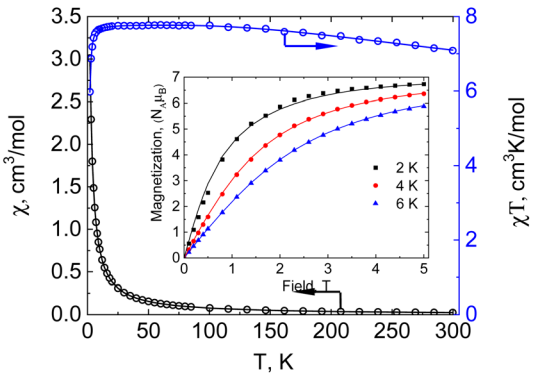

Fig. 2 Temperature dependence of χT for **1** measured at H_{DC} = 5000 Oe. Inset: magnetization *vs.* field for **1** measured at T = 2, 4 and 6 K. Theoretical curves (solid lines) are calculated with $J_{Mn1-Mn2}$ = +67.3(3) cm^{-1}, $g_{iso(Mn1)}$ = 1.960(8), $g_{iso(Mn2)}$ = 1.998(3), D_{Mn2} = −0.727(8) cm^{-1}, zJ' = −0.00321(12) cm^{-1}.

observed at 300 K. Upon lowering of the temperature, χT increases steadily and reaches a maximum value of 7.78 cm^3 K mol^{-1} at 60 K and then decreases to 7.70 cm^3 K mol^{-1} at *ca.* 14 K and drops down to 5.98 cm^3 K mol^{-1} at 2 K. Such behaviour supports significant ferromagnetic exchange between spin centres. The field dependence of magnetization (in the range 0–5 T) was measured at 2, 4 and 6 K (see the inset in Fig. 2). Measured at 2 K the magnetization is $6.73 N_A \mu_B$ at 5 T, close to the saturation value of 7 $N_A\mu_B$, supporting the $S = 7/2$ spin of the ground state for compound **1**. The temperature dependence of magnetic susceptibility and the field dependence of magnetization were simultaneously fitted by the PHI program,[28] assuming a three spin system – two with one unpaired electron and one with five. For the two terminal Mn1 and Mn1′ ions the isotropic g-factor was considered the same due to symmetry relation and different from the g-factor of the middle Mn2. Exchange interactions between Mn2 and Mn1 (Mn1′) centres were considered as equal, $J_{Mn1-Mn1'}$ was arbitrarily taken to be zero. So, the spin Hamiltonian was taken as: $\hat{H} = 2J_{Mn1-Mn2}(\hat{S}_{Mn1}\hat{S}_{Mn2} + \hat{S}_{Mn1'}\hat{S}_{Mn2})$. The molecular field zJ' was considered. Addition of axial anisotropy parameter D on the Mn2 appeared to be essential for accurate description of the field magnetization dependence, especially at 2 K. A graphical representation of experimental data and fitted dependencies is given in Fig. 2. A very nice description of the experimental data is obtained with $J_{Mn1-Mn2}$ = +67.3(3) cm^{-1}, $g_{iso(Mn1)}$ = 1.960(8), $g_{iso(Mn2)}$ = 1.998(3), D_{Mn2} = −0.726(8) cm^{-1}, zJ' = −0.00321(12) cm^{-1} (residual value R = 0.0054). So, very strong ferromagnetic exchange (extremely unusual for Mn–Mn exchange coupling) interaction determines the ground spin state of 7/2 in **1**.

Unprecedented Mn···Mn ferromagnetic coupling and uncertainty in explanation of the structural data led us to the idea to perform DFT calculations (PBE0/6-311G(d) level of theory) of **1** and the corresponding $[MnL_3]^-$ anionic unit (see computational details in the ESI†). For the ground $S = 7/2$ state of **1** a very interesting spin density (SD) distribution was found (see Fig. 3, left). SD of spin-up (α) electrons is located on the metal centres while there is significant spin-down (β) SD on the bridging NO moieties (values of calculated Mulliken SD and charge are shown in Table 1). Such SD distribution in the trinuclear compound is inherited from the isolated $[MnL_3]^-$ unit in the $S = 1/2$ state (see Fig. 3, right), in which a spin-polarized electronic distribution is observed, not accompanied by charge polarization.

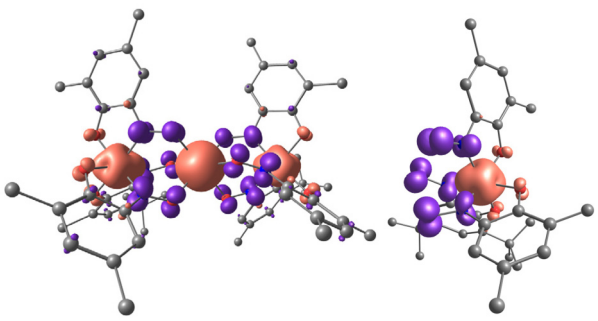

Fig. 3 Spin density (SD) distribution in compound **1** (left) and isolated anionic fragment $[MnL_3]^-$ (right). Methyl groups and hydrogen atoms are omitted for clarity. Red coloured surface – positive SD, blue – negative, contour value 0.01 e Å^3 (PBE0/6-311G(d) level of theory).

Table 1 Mulliken charge (q, e) and spin density (ρ, e) distribution on Mn centres, ligand **L** (summed over all atoms) and bridging NO groups in compound **1** (PBE0/6-311G(d))

Unit	q	ρ
Mn1	1.465	2.363
Mn2	1.520	4.728
L	−0.742	−0.414
3L [a]	−2.226	−1.242
NO	−0.807	−0.387

[a] Total quantity for three **L** ligands.

In compound **1** on the central Mn2 (which is undoubtedly in the +2 oxidation state) the Mulliken charge is +1.520, while the charge on the Mn1 and Mn1′ ions is +1.465, even less positive than for the Mn2 ions. Each ligand gains only 0.414 of β-SD which is predominantly located on the NO bridges (0.387 of β-SD). The total Mulliken charge on each ligand is only $-0.742e$. Thus, the calculated Mulliken charge and SD distribution for **1** is very far from described by the mesomeric formula $[\{Mn^{IV}(L^{2-})_2(L^-)\}Mn^{II}\{Mn^{IV}(L^{2-})_2(L^-)\}]$ with a formal +4 Mn oxidation state of the terminal Mn ions and dianion radical structure for two of the three ligands in $[ML_3]^-$ (with formal minus five charge and two unpaired electrons distributed evenly over three ligands). Also the $\{[Mn^{II-LS}L_3]Mn^{II-HS}[Mn^{II-LS}L_3]\}$ mesomeric structure is not fully supported. The spin-polarized LS state of the $[MnL_3]^-$ with SD on Mn1 (Mn1′) +2.363 and total opposite sign SDs on the three ligands of −1.242 is observed. So, the actual electronic distribution is in between these two polar mesomers, closer to the latter.

For the $[MnL_3]^-$ unit the relative energies of states with total spin S = 1/2, 3/2 and 5/2 were calculated to be 0.0, 6277 and 12 271 cm^{-1}, respectively, proving its local LS ground state.

The unusual highly spin-polarized state of $[MnL_3]^-$ is obviously the reason for strong ferromagnetic spin alignment of the metal spin centres. Formally it can be described as mediated by antiferromagnetic interaction of the ligand β-SD (located on NO bridging groups) with the Mn1 and Mn2 metal centres.

So, we tested an alternative description of the magnetochemistry data considering a five spin-centre system: $S_{Mn1} = S_{Mn1'} = 3/2$, $S_{GL} = S_{GL'} = 1$ (fictious centres GL and GL′ describe spin density on the group molecular orbitals of the $\mathbf{L_3}$ units involving NO moieties with two unpaired electrons) and S_{Mn2} = 5/2 with the following spin Hamiltonian: $\hat{H} = 2J_{Mn1\text{-}GL}(\hat{S}_{Mn1}\hat{S}_{GL} + \hat{S}_{Mn1'}\hat{S}_{GL'}) + 2J_{Mn2-GL}(\hat{S}_{Mn2}\hat{S}_{GL} + \hat{S}_{Mn2}\hat{S}_{GL'})$. For all spin centres an isotropic g factor was considered, for GL (GL′) centres g was fixed at 2.0 to avoid overparameterization. D was varied for the terminal Mn centres. The set of the

best fit parameters was found to be the following: $g_{Mn1} = g_{Mn1'} = 1.9797(10)$; $g_{Mn2} = 2.0061(13)$; $D_{Mn1} = D_{Mn1'} = -1.561(10)$ cm^{-1}; $zJ' = -0.00326(10)$ cm^{-1}; $J_{Mn1-GL} = -240.5(7)$ cm^{-1}; $J_{Mn2-GL} = -219(3)$ cm^{-1} (residual sum is $R = 0.0052$). The quality of the fit is the same as for the three spin centres description, and the fitted g-factors for the Mn1 and Mn2 centres and zJ' values are rather close. The extremely strong ferromagnetic exchange interaction with $J_{Mn1-Mn2} = +67.3(3)$ cm^{-1} in the case of the three-spin system is replaced by two strong antiferromagnetic exchange interactions of fictious ligand spin centres GL with Mn1 ($J_{Mn1-GL} = -240.5(7)$ cm^{-1}) and Mn2 ($J_{Mn2-GL} = -219(3)$ cm^{-1}) metal centres, resulting in the same $S = 7/2$ ground spin state.

ac magnetic measurements were initially performed at 2 K at zero and applied external magnetic field. At zero field no out-of-phase signal is registered for **1**, application of the field leads to development of the out-of-phase signal (Fig. S4, ESI†). The optimal value of dc field was $H_{DC} = 2500$ Oe and ac susceptibility measurements were performed at this field. The frequency dependence of the imaginary part of ac susceptibility is shown in Fig. 4, and both components of the dynamic magnetic susceptibility are presented in Fig. S5, ESI.† Relaxation times were plotted against the inverse of temperature and fitted with the theoretical expressions for different relaxation mechanisms and their combination (Fig. 5).

The nonlinear course of this dependence evidences the contribution of non-Orbach relaxation mechanisms. The temperature dependence of the relaxation times *vs.* the inverse of temperature was nicely fitted ($R^2 = 0.998$) with the sum of two contributions – from a Raman process $\tau_{Raman}^{-1} = C_{Raman}T^n$ and quantum tunnelling of magnetization (QTM, $\tau_{QTM}^{-1} = B$) (red solid line in Fig. 5). The obtained best-fit parameters of the relaxation processes are $C_{Raman} = 390(40)$ K^{-n} s^{-1}, $n = 1.78(5)$, and $B = 1.74(10) \times 10^3$ s^{-1}.

Approximation of the high-temperature part of the temperature dependence of the relaxation time with the Arrhenius law (blue dotted line in Fig. 5) gives an effective magnetization reversal barrier of $U_{eff}/k_B = 34(2)$ K and $\tau_0 = 2.4(3) \times 10^{-6}$ s.

In conclusion, a linear homotrinuclear manganese heterospin complex with $S = 7/2$ ground state showing field induced slow magnetization relaxation was synthesized. Terminal $[MnL_3]^-$ units are in a local $S = 1/2$ state, the central Mn(II) ion is in a HS ($S = 5/2$) state. Spin polarization in $[MnL_3]^-$ with partial β-spin density on bridging NO groups is determining the strong ferromagnetic interaction between Mn ions ($J_{Mn1-Mn2} = +67.3(3)$ cm^{-1}).

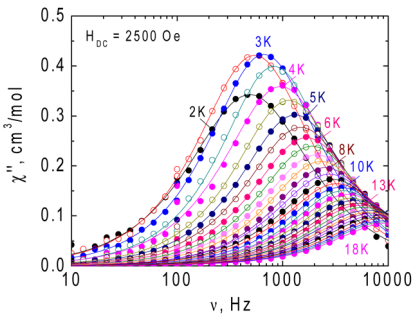

Fig. 4 Frequency dependence of the imaginary component (χ'') of dynamic magnetic susceptibility for **1** in the range 2–18 K at a dc supporting magnetic field of $H_{DC} = 2500$ Oe. Solid lines are approximations of the experimental data using a generalized Debye model.

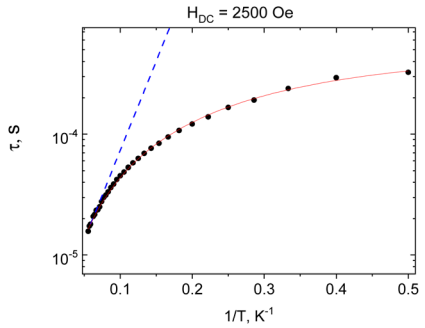

Fig. 5 Dependence of the relaxation time and the inverse of temperature $\tau(1/T)$ of **1** ($H_{DC} = 2500$ Oe). Blue dotted line – approximation of the high temperature part by the Arrhenius law. Red solid line – approximation by the sum of Raman and QTM-type contributions. Black circles – experimental data.

Conflicts of interest

There are no conflicts to declare.

Acknowledgements

This research was supported by the Russian Science Foundation (project no. 22-23-00956). N. N. E. thanks the state assignment of the IGIC RAS in the field of fundamental scientific research for magnetic measurements at the JRC PMR IGIC RAS.

References

1 O. Kahn, *Molecular Magnetism*, VCH Publishers, New York, 1993.
2 R. Sessoli, D. Gatteschi, A. Caneschi and M. A. Novak, *Nature*, 1993, **365**, 141–143.
3 V. V. Lukov, V. A. Kogan, S. I. Levchenkov, I. N. Shcherbakov and L. D. Popov, *Russ. J. Coord. Chem.*, 2015, **41**, 1–15.
4 D. Gatteschi, *Adv. Mater.*, 1994, **6**, 635–645.
5 E. Coronado, *Nat. Rev. Mater.*, 2020, **5**, 87–104.
6 F. Troiani and M. Affronte, *Chem. Soc. Rev.*, 2011, **40**, 3119–3129.
7 M. N. Leuenberger and D. Loss, *Nature*, 2001, **410**, 789–793.
8 L. Bogani and W. Wernsdorfer, *Nat. Mater.*, 2008, **7**, 179.
9 R. Sessoli, D. Gatteschi, A. Caneschi and M. Novak, *Nature*, 1993, **365**, 141.

10 A. Caneschi, D. Gatteschi, R. Sessoli, A. L. Barra, L. C. Brunel and M. Guillot, *J. Am. Chem. Soc.*, 1991, **113**, 5873–5874.
11 G. A. Craig and M. Murrie, *Chem. Soc. Rev.*, 2015, **44**, 2135–2147.
12 S. Gómez-Coca, D. Aravena, R. Morales and E. Ruiz, *Coord. Chem. Rev.*, 2015, **289–290**, 379–392.
13 J. M. Frost, K. L. M. Harriman and M. Murugesu, *Chem. Sci.*, 2016, **7**, 2470–2491.
14 R. Mičová, C. Rajnák, J. Titiš, E. Samoľová, M. Zalibera, A. Bieńko and R. Boča, *Chem. Commun.*, 2023, **59**, 2612–2615.
15 T. T. da Cunha, V. M. M. Barbosa, W. X. C. Oliveira, E. F. Pedroso, D. M. A. García, W. C. Nunes and C. L. M. Pereira, *Inorg. Chem.*, 2020, **59**, 12983–12987.
16 K. Uchida, G. Cosquer, K. Sugisaki, H. Matsuoka, K. Sato, B. K. Breedlove and M. Yamashita, *Dalton Trans.*, 2019, **48**, 12023–12030.
17 C. Rajnák, J. Titiš, J. Moncol, R. Mičová and R. Boča, *Inorg. Chem.*, 2019, **58**, 991–994.
18 X.-L. Li, F.-Y. Min, C. Wang, S.-Y. Lin, Z. Liu and J. Tang, *Dalton Trans.*, 2015, **44**, 3430–3438.
19 I. Oyarzabal, A. Zabala-Lekuona, A. J. Mota, M. A. Palacios, A. Rodríguez-Diéguez, G. Lorusso, M. Evangelisti, C. Rodríguez-Esteban, E. K. Brechin, J. M. Seco and E. Colacio, *Dalton Trans.*, 2022, **51**, 12954–12967.
20 E. Pilichos, P. Bhunia, M. Font-Bardia, A. Ghosh, J. Mayans and A. Escuer, *Dalton Trans.*, 2022, **51**, 1779–1783.
21 A. M. Ionov, S. N. Lyubchenko, V. A. Kogan and A. Y. Tsivadze, *Russ. J. Coord. Chem.*, 2008, **34**, 195–197.
22 S. N. Lyubchenko, A. M. Ionov, I. N. Shcherbakov, G. G. Aleksandrov, V. A. Kogan and A. Y. Tsivadze, *Russ. J. Coord. Chem.*, 2006, **32**, 539–544.
23 I. I. Krotkii, E. Y. Shcherbakova, S. N. Lyubchenko, N. N. Efimov, M. A. Kiskin, V. A. Lazarenko, P. A. Knyazev, S. P. Kubrin, G. S. Borodkin and I. N. Shcherbakov, *Polyhedron*, 2024, **251**, 116876.
24 S. Chattopadhyay, P. Basu, S. Pal and A. Chakravorty, *J. Chem. Soc., Dalton Trans.*, 1990, 3829–3833.
25 D. N. Hendrickson and C. G. Pierpont, *Valence Tautomeric Transition Metal Complexes in Spin Crossover in Transition Metal Compounds II*, Springer Berlin Heidelberg, Berlin, Heidelberg, 2004, pp. 63–95, DOI: **10.1007/b95413**.
26 M. W. Lynch, D. N. Hendrickson, B. J. Fitzgerald and C. G. Pierpont, *J. Am. Chem. Soc.*, 1981, **103**, 3961–3963.
27 S. N. Brown, *Inorg. Chem.*, 2012, **51**, 1251–1260.
28 N. F. Chilton, R. P. Anderson, L. D. Turner, A. Soncini and K. S. Murray, *J. Comput. Chem.*, 2013, **34**, 1164–1175.